ANALYSIS OF fMRI DATA USING SPLINE WAVELETS

Manuela Feilner, Thierry Blu and Michael Unser
Biomedical Imaging Group, IOA/DMT
Swiss Federal Institute of Technology Lausanne
CH-1015 Lausanne EPFL
Switzerland
e-mail: manuela.feilner@epfl.ch

ABSTRACT

Our goal is to detect and localize areas of activation in the brain from sequences of fMRI images. The standard approach for reducing the noise contained in the fMRI images is to apply a spatial Gaussian filter which entails some loss of details. Here instead, we consider a wavelet solution to the problem, which has the advantage of retaining high-frequency information. We use fractional-spline orthogonal wavelets with a continuously-varying order parameter α; by adjusting α, we can balance spatial resolution against frequency localization. The activation pattern is detected by performing multiple (Bonferroni-corrected) t-tests in the wavelet domain. This pattern is then localized by inverse wavelet transform of a thresholded coefficient map.
In order to compare transforms and to select the best α, we devise a simulation study for the detection of a known activation pattern. We also apply our methodology to the analysis of acquired fMRI data for a motor task.

1 INTRODUCTION

Motor and cognitive tasks induce neuronal activation in specific locations in the brain. This neuronal activation involves local changes in the cerebral blood oxygenation which can be measured by a scanner, through a spin resonance technique. This non-invasive detection of blood-oxygenation-level-dependent contrast (BOLD) by fMRI offers new possibilities for neurophysiologists and gives better insights into the functionality of the human brain [1]. Images taken under different conditions are processed in order to find the activation loci. The practical difficulty is that the signal changes are very small and the noise is relatively high. This noise has two distinct origins: noise due to physiological activities (e.g., cardiac [2], respiratory motions, task/stimulus related motions), [3, 4] and noise of the measurement instrument (e.g., scanner) [5].
Head motion cannot be completely avoided either. Motion may produce signal changes of the same order of magnitude as the fMRI BOLD effects [6]. This calls for the use of accurate image-registration algorithms in a preprocessing stage [7].

The standard technique for performing the analysis of fMRI data is SPM (Statistical Parameter Mapping) [8]. This software package is available freely and is widely used by researchers in the field. SPM, however, has some limitations [9]. It applies a spatial Gaussian filter to the data which entails a loss of resolution. This filtering correlates the data, which makes the statistical analysis intricate; pixels no longer remain independent. Finally, the statistical inference in SPM is based on the theory of continuous Gaussian random fields [10, 11]; it is mathematically complex and not entirely adequate, because the data to which it is applied is discrete while the theory is continuous.

Here, we consider using a wavelet transform approach as proposed in [12]. The advantages are twofold. First, we don't loose any signal details. Second, we don't introduce any correlations, provided that we use an orthogonal transform. We apply the wavelet transform to the difference images $I_{D_\tau}(x,y) = I_{A_\tau}(x,y) - I_{B_\tau}(x,y)$, where the symbols A and B correspond to the two distinct experimental conditions (block paradigm), and where τ is the time index (sequence of realizations).

Because of the noise present in the data, it is almost impossible to detect any activation without resorting to statistical analysis. This analysis requires a modelisation of noise [13]; here, we assume that $I_{D_\tau}(x,y)$ follows a spatio-temporal Gaussian distribution. Thanks to the wavelet transform, we can apply simple statistics, which makes the analysis fast. The present study proposes two improvements to the method of Ruttimann et al. [12]: (i) It uses t-statistics instead of z-scores and thus does not require the hypothesis of stationary noise made previously, (ii) It uses a new class of fractional-spline wavelets, which allows for a finer tuning of the transform (continuously-varying order parameter).

The paper is organized as follows: In Section 2, we present the algorithm and describe our new wavelet transform. In Section 2.2, we present our statistical analysis method which detects the activation area in the

wavelet domain. In Section 2.4.1, we shortly describe the fMRI-data. In Section 2.4, we present our evaluation and comparison procedure. Finally, in Section 3, we present experimental results with both simulated and real fMRI data.

2 Algorithm Proposal

Due to their high level of noise, the fMRI images must be processed in the space domain prior to averaging. Here, we want to avoid the standard smoothing technique because it would suppress fine-resolution details. Thus, we apply a Discrete Wavelet Transform (DWT) to $I_{D_\tau}(x,y)$ (spatial data) to get the decomposed fMRI-data $I_{W_\tau}(x,y)$ (W-data, where "W" stands for "Wavelet Domain"), as described below. Note that the Gaussian hypothesis for the noise is preserved in the W-domain. Then, we apply a classical statistical testing on the W-data (see Subsection 2.2). Based on the outcome of the local t-test, we apply an adaptive threshold in the wavelet domain. This yields the W-estimated activation $I_{\text{est,W}}(x,y)$ (WEA). We apply the inverse DWT on the WEA, and subsequently quantize the resulting image (see Subsection 2.3). Finally, we obtain the estimated activation in the space domain $I_{\text{est}}(x,y)$ (SEA) by identifying the pixel values above the residual noise level.

2.1 Structure Proposal: Wavelet Transform

We propose to transform the data using an iterated orthogonal filterbank, whose analysis version is depicted in Figure 1 and whose synthesis version is depicted in Figure 2. In Figure 1, due to orthogonality, we have that $\widetilde{H}(z) = H(\frac{1}{z})$ and that $\widetilde{G}(z) = G(\frac{1}{z})$. More specifically, we are going to use filters that generate fractional-spline scaling functions and wavelets.

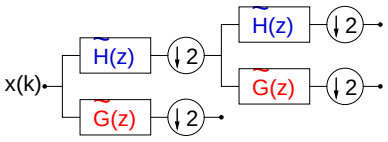

Figure 1: Analysis part of the wavelet transform (DWT), where the input x is one line of I_{D_τ}.

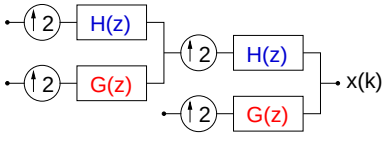

Figure 2: Synthesis part of the wavelet transform (IDWT)

2.1.1 The Fractional-Spline Transform

β_+^α is the causal fractional-spline of degree α, which is a linear combination of the one-sided power function $(x-n)_+^\alpha$. In the frequency domain we get $\hat{\beta}_+^\alpha(\omega) = \left(\frac{1-e^{-j\omega}}{j\omega}\right)^{\alpha+1}$. The symmetric fractional-spline (β_*^α) is a linear combination of $|x-n|_+^\alpha$, if α is not an even integer. If α is an even integer, β_*^α is a linear combination of $|x-n|_+^\alpha \log|x-n|$. In the frequency domain, we obtain $\hat{\beta}_*^\alpha(\omega) = \left|\frac{1-e^{-j\omega}}{j\omega}\right|^{\alpha+1}$. The autocorrelation filter of a B-spline of degree α is given by $A^\alpha(e^{j\omega}) = \sum_n \left|\hat{\beta}_*^\alpha(\omega+2n\pi)\right|^2$. We denote the Fourier transform of the orthogonalized symmetric fractional-spline by $\hat{\beta}_{*\text{ortho}}^\alpha(\omega) = \frac{\hat{\beta}_*^\alpha(\omega)}{\sqrt{A^\alpha(e^{j\omega})}}$ [14]. The corresponding lowpass filter is given by $H_*^\alpha(z) = \sqrt{2}\left|\frac{1+z^{-1}}{2}\right|^{\alpha+1}\sqrt{\frac{A^\alpha(z)}{A^\alpha(z^2)}}$, and the highpass filter is given by $G_*^\alpha(z) = \frac{1}{z}H_*^\alpha\left(-\frac{1}{z}\right)$. For the causal case we get $H_+^\alpha(z) = \sqrt{2}\left(\frac{1+z^{-1}}{2}\right)^{\alpha+1}\sqrt{\frac{A^\alpha(z)}{A^\alpha(z^2)}}$ and $G_+^\alpha(z) = \frac{1}{z}H_+^\alpha\left(-\frac{1}{z}\right)$, where $z = e^{j\omega}$.

Since for $\alpha > -\frac{1}{2}$ the fractional-splines satisfy all the requirements for a multiresolution analysis of L^2, they can be used to build families of wavelet bases with a continuously-varying order parameter [15]. By varying α, we can trade spatial localization (small α) for frequency localization (large α). As $\alpha \to +\infty$, the wavelets tend to ideal filters (Shannon wavelets) which are maximally localized in frequency but have poor spatial decay. Note that β_{+ortho}^0 is equivalent to the Haar function, while β_{*ortho}^0 is not.

2.2 Activation Detection by Statistical Testing on WDC

The subsequent analysis is done at the coefficient level, where $I_{W_\tau}(x,y)$ denotes any wavelet-coefficient at a certain time τ.

2.2.1 Hypothesis testing

To decide which coefficient is activated, we use hypothesis testing. We denote the null hypothesis—the pixel under consideration is not activated—by H_0. Under this hypothesis, $\mathrm{E}\{I_W(x,y)\} = 0$, where $I_W(x,y) = \frac{1}{n}\sum_t I_{W_t}(x,y)$ (n is the total number of realizations), and the distribution for the mean value of each coefficient relative to its standard deviation is known (t-distribution), see 2.2.2. If a coefficient exceeds some expected bound for I_W, the null hypothesis is rejected and the alternative hypothesis H_1 is accepted; we conclude that the pixel is activated. The decision is made by setting a threshold.

Given some probability value α', we compute the threshold T such that the probability that a normalized version (t-value) of $I_W(x,y)$ exceeds T is less than or equal to α', assuming that H_0 is true. In other words,

α' is the probability of observing values higher than T by chance, given that the null hypothesis is true. This probability α' is called the *level of significance* of the test. When a coefficient exceeds this threshold, we reject the null hypothesis and accept the alternative hypothesis H_1.

1. Null hypothesis H_0: $\mathrm{E}\{I_W(x,y)\} = 0$ (no activation);
2. Alternative hypothesis H_1: $\mathrm{E}\{I_W(x,y)\} \neq 0$ translates into $I_W(x,y) \geq T$, where T is a significance threshold as explained in Section 2.2.3.

2.2.2 Choosing the Test Statistic

The p-value is the probability of obtaining a test statistic at least as extreme as the one we observed, given that the null hypothesis is true. The smaller the p-value, the stronger the evidence against H_0.
The test on the distribution has to be adapted to the set of data, which transforms the wavelet values into p-values.

In a previous work [13], we found the noise variance to vary over space, contrary to what has often been assumed in the literature [12].
Since the variance σ^2 changes over space, we can renormalize the noise by computing the test statistic

$$t(x,y) = \frac{I_W(x,y)}{\frac{s_W(x,y)}{\sqrt{n}}}, \qquad (1)$$

where $s_W(x,y)^2 = \frac{1}{n-1}\sum_{\tau=1}^{n}(I_{W_\tau(x,y)} - I_W(x,y))^2$. This t-value is now voxel-independent and follows Student's t-distribution. Its realizations can thus be tested using Student's t-test.

2.2.3 Determining Significance Levels

When we consider all wavelet coefficients jointly, we have to correct for multiple testing. Since we don't want to have globally more than $\alpha'\%$ of wrong activation decisions, we have to divide α' by the total number of coefficients. This is known as the Bonferroni-correction for multiple testing: $\alpha'' = \alpha'/N$, where N is the number of wavelet coefficients in the image. This corrected value is known to be conservative; it can eventually be decreased if there is correlation in the data. In our case, however, we are keeping correlation low by working in the wavelet domain, in contrast with Gaussian smoothing which introduces significant dependencies.

2.3 Quantization

The original fMRI data are always quantized. We thus quantize the estimated activation $I_{\mathrm{est}}(x,y)$ using the same quantization levels. This localizes the fractional-spline filters which are, in general, of infinite length. Also, due to the amount of noise that is present in the data, it is necessary to threshold the data proportionaly to the noise level. More specifically, if the noise on every realization has a standard deviation of σ, we choose a threshold level of $\sigma\sqrt{2/n}$, which corresponds to the noise level of the average image $I_D(x,y) = \frac{1}{n}\sum_\tau I_{D_\tau}(x,y)$.

2.4 Quality measurements

2.4.1 Description of our fMRI-Data

In this study, we investigate simple fMRI block paradigms. This set of fMRI data consists of 8 repetitions of alternating blocks, according to distinct experimental conditions: brain volume with activation, left-hand finger tapping, and brain volume in the rest state. Each block contains 3 acquisitions. In our case, a full volume of 30 slices of 128×128 pixels each was acquired every 6 seconds.
The expected activation is roughly an ellipse in a well-defined part of the right hemisphere of the brain (motor cortex).

2.4.2 Test image

To optimize the structural wavelet parameters (degree α and depth of decomposition J) we used different test images $I(x,y)$, where we knew the activated area A, defined as $\{(x,y)|I(x,y) \neq 0\}$. The complementary region A^c is defined by $\{(x,y)|I(x,y) = 0\}$. We used thresholded ellipse-shaped Gaussian activation patterns. The test-data were generated by adding white Gaussian noise (20 realizations for the activated state, and 20 noise-only realizations for the resting state). We changed several parameters such as the scale and ellipticity of the ellipse, its orientation and position, the amplitude of the noise.

2.4.3 Quality measure E

We counted the number of false detections (i.e., errors type I (E1) defined by $E1 = \mathrm{Card}(\{(x,y) \in A^c | I_{\mathrm{est}}(x,y) \neq 0\})$ and the number of missed detections (i.e., errors type II (E2), $E2 = \mathrm{Card}(\{(x,y) \in A | I_{\mathrm{est}}(x,y) = 0\})$ pixels). We defined the quality measure $E = E1 + E2$. This measurement controles the estimation of the activation zone, but does not take the amplitude into account. For the optimization, we minimized E with respect to the structure parameter (α and J).

3 Results

The first example presented in Figure 3 is the statistical average of a simulation experiment using an elliptic shape approximating the expected activation pattern in the motor task described in Subsection 2.4.1. We chose an SNR of -1.7 dB corresponding to the noise on our real fMRI data. We optimized the wavelet transform for the following parameters in the case of the fractional-spline transform: degree $\alpha \in [-0.2, ..., 6]$, type symmetric or causal, iteration depth $J = 1, 2, 3$; and in the case of Daubechies wavelets: order 1 to 7, iteration depth $J = 1, 2, 3$. We observe that, in this specific experiment, the

symmetric fractional-spline transform yields the best results (i.e., the smallest error E). The minimum, which is attained for $\alpha = 1.2$ and $J = 1$, is quite pronounced (see Figure 3 left). In comparison, the Daubechies transform yields results that are twice worse. More specifically, we find that $\min(E)_* < \min(E)_+ < \min(E)_{\text{Daubechies}}$.

We then used this optimal α to detect activation in one slice of real data (see Figure 3 right): the detected shape is in good agreement with the anatomy. Moreover, we found our optimized wavelet approach to yield significantly fewer false activations than the other methods (correlation methods, SPM Gaussian filter). We also tested our algorithm on other fMRI data, generated by a visual task, performed by various volunteers; the obtained results were quite encouraging as well.

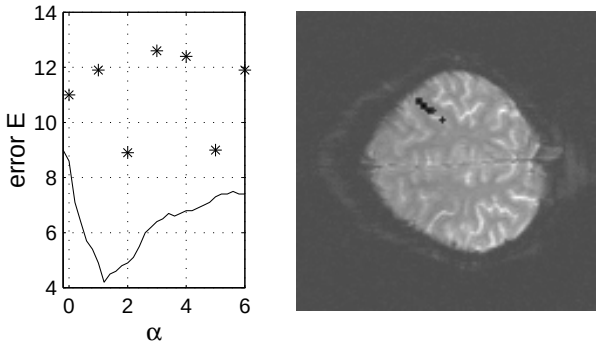

Figure 3: Simulated data (left): plot of the average detection error E, as a function of the symmetric spline degree α (plain line), and as a function of the Daubechies filter order (stars); Real data (right): detection of the activation (black pixels) found in one transverse fMRI slice for the experiment described in Subsection 2.4.1.

4 Conclusion

We described a wavelet based algorithm for detecting activation in fMRI data. For this purpose, we applied a new wavelet transform: the fractional-spline transform. We showed that it was possible to optimize the transform with respect to its continuous parameter, the degree α of the spline. We tested our algorithm on simulated data, as well as on real fMRI images.

With our method we can detect different shapes with different sizes and we observe that this technique is very robust with respect to noise. The optimization of the structure parameters in our algorithm improves the accuracy of the detection. Future work will concentrate on optimizing the wavelet structure parameters when the activation pattern is not known a priori. Also, this 2-D method can be straightforwardly extended to 3-D, in order to take into account the volumic structure of fMRI data.

Acknowledgments

We thank Arto Nirkko from Inselspital in Bern for providing the fMRI data. This work was supported in part by the Swiss National Science Foundation under grant 2100-053540.

References

[1] S. Ogawa, R. Menon, D. Tank, S. Kim, H. Merkle, J. Ellerman, and K. Ugurbil, "Functional brain mapping by blood oxygenation level-dependent contrast magnetic resonance imaging," *Biophysical J.* **64**, pp. 803–812, 1993.

[2] M. Dagli, J. Ingeholm, and J. Haxby, "Localization of cardiac-induced signal change in fMRI," *NeuroImage* **9**, pp. 407–415, 1999.

[3] E. Bullmore, M. Brammer, S. Rabe-Hesketh, V. Curtis, R. Morris, S. Williams, T. Sharma, and P. McGuire, "Methods for diagnosis and treatment of stimulus-correlated motion in generic brain activation studies using fMRI," *Human Brain Mapping* **7**, pp. 38–48, 1999.

[4] S. Ogawa, R. Menon, S. Kim, and K. Ugurbil, "On the characteristic of functional magnetic resonance imaging of the brain," *Annu. Rev. Biophys.* **27**, pp. 447–474, 1998.

[5] T. Budinger, F. Wehrli, *et al.*, *Mathematics and Physics of Emerging Biomedical Imaging*, National Academic Press, 1996.

[6] R. Cox, "A two day workshop on functional MRI," in *Proc. Colloque de Physique C2*, June 1996.

[7] P. Thevenaz, U. Ruttimann, and M.Unser, "A pyramid approach to subpixel registration based on intensity," *IEEE Trans. Image Processing* **7**(1), pp. 27–41, 1998.

[8] R. Frackowiak, K. Friston, C. Frith, R. Dolan, and J. Mazziotta, *Human Brain Function*, Academic Press, 1997.

[9] S. Gold, B. Christian, S. Arndt, G. Zeien, T. Cizadlo, D. Johnson, M. Flaum, and N. Andreasen, "Functional MRI statistical software packages: A comparative analysis," *Human Brain Mapping* **6**, pp. 73–84, 1998.

[10] K. Worsley, "Local maxima and the expected Euler characteristic of excursion sets of ξ^2, t and f fields.," *Journal of Applied Probability* **26**, pp. 13–42, 1994.

[11] K. Worsley, A. Evens, S. Marrett, and P. Neelin, "A three dimensional statistical analysis for cbf activation studies in human brain.," *J. Cerebral Blood Flow and Metabolism* **12**, pp. 900–918, 1992.

[12] U. Ruttimann, M. Unser, R. Rawlings, D. Rio, N. Ramsey, V. Mattay, D. Hommer, J. Frank, and D. Weinberger, "Statistical analysis of functional MRI data in the wavelet domain," *IEEE Trans. Medical Imaging* **17**(2), pp. 142–154, 1998.

[13] M. Feilner, T. Blu, and M. Unser, "Statistical analysis of fmri data using orthogonal filterbanks," *SPIE*, 1999.

[14] T. Blu and M. Unser, "The fractional spline wavelet transform: Definition and implementation," in *Proc. ICASSP*, (Istanbul, Turkey), June 2000.

[15] M. Unser and T. Blu, "Fractional splines and wavelets," *SIAM Review* **42**, pp. 43–67, 2000.